

# The Role of HfO<sub>2</sub>/SiO<sub>2</sub> Thin-Film Interfaces in Near-Ultraviolet Absorption and Pulsed-Laser Damage

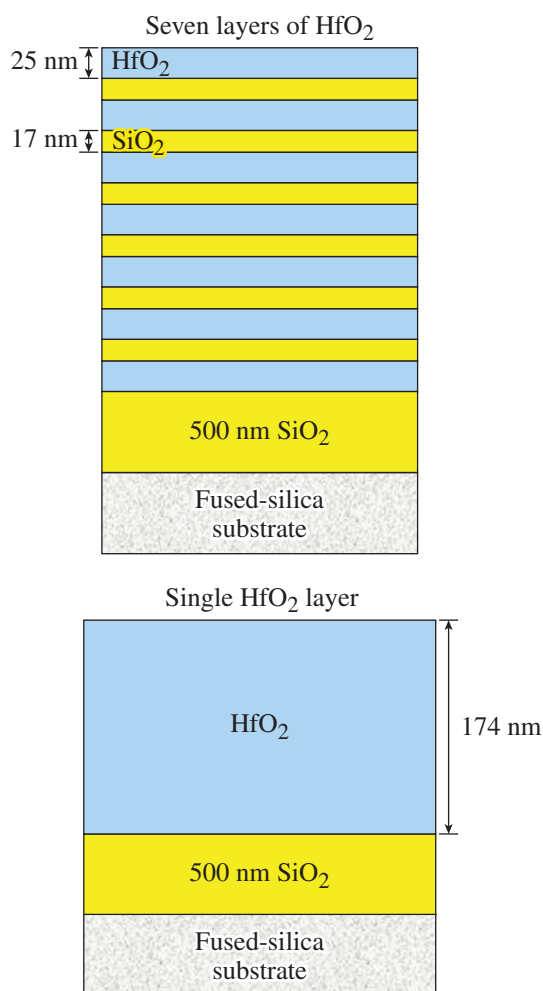
## Introduction

It has been well established that nanosecond-pulse laser damage of multilayer coatings comprised of HfO<sub>2</sub>/SiO<sub>2</sub> pairs in the near-ultraviolet (near-UV) spectral range is initiated in the high-index HfO<sub>2</sub> component of the coating. Still, very limited information about optical and structural properties of interfacial areas between layers renders interfaces as a probable source of enhanced absorption and damage. The reduced E-field design,<sup>1</sup> which moves intensity peaks away from interfaces into the more-damage-resistant SiO<sub>2</sub> layer, frequently improves damage threshold<sup>2</sup> but does not clarify the role of interfaces in laser damage. The only (to our knowledge) study<sup>3</sup> directly addressing interface absorption and its role in pulsed laser damage used a 1064-nm laser wavelength, with e-beam-deposited metal oxides (including HfO<sub>2</sub>) and SiO<sub>2</sub> as high- and low-index materials, respectively. In that study, based on comparative absorption and damage-threshold measurements for half-wave stacks with numerous interfaces and a single-layer high-index material, HfO<sub>2</sub>/SiO<sub>2</sub> interfaces made a significant contribution to total absorption and produced lower damage thresholds compared to a single HfO<sub>2</sub> layer. In this work a similar approach is used, but with different coatings designs, to study the contribution of HfO<sub>2</sub>/SiO<sub>2</sub> interfaces to absorption in the near-UV and their role in the nanosecond-pulse damage initiation. One of the study goals is to explore how interfaces perform in coatings with different porosity and packing density. For this purpose the coatings were deposited using two techniques: (1) conventional electron-beam evaporation, typically producing rather porous films, and (2) ion-beam sputtering, which creates very densely packed films with sharp interfaces.<sup>4</sup> Despite the difference in thin-film structure, we found that in both cases the interfaces contribute insignificantly to total absorption and are not the main source of damage initiation.

## Experimental

The coatings containing HfO<sub>2</sub> and SiO<sub>2</sub> materials were manufactured using either e-beam evaporation with a rate of 1.2 Å/s and 4.6 Å/s for HfO<sub>2</sub> and SiO<sub>2</sub>, respectively, and an oxygen backfill pressure of  $2 \times 10^{-4}$  Torr, or reactive ion-beam sputtering, with no assist ion gun, and post-deposition annealing at 300°C for 8 h. The two types of coating samples—single

HfO<sub>2</sub> layer and HfO<sub>2</sub>/SiO<sub>2</sub> multilayer—were manufactured using a design shown schematically in Fig. 145.42. In the case of e-beam deposition, both samples were prepared in a single vacuum cycle run using shutters beneath the single-layer sample during thin SiO<sub>2</sub> layer deposition. This approach ensured that exactly the same HfO<sub>2</sub> material and deposition conditions were used for either film formation. The ion-beam-sputtered



G10628JR

Figure 145.42 Schematic of the film containing seven HfO<sub>2</sub> layers separated by narrow SiO<sub>2</sub> layers and a single layer of HfO<sub>2</sub> film.

coatings were prepared in two separate coating depositions because of hardware limitations. Based on the high reproducibility of the sputtered-coating optical parameters measured for a number of runs, we anticipate that it should not affect the outcome of the experiment.

It is important to note here that a comparative laser-damage study imposes a few stringent requirements on the thin-film design and the resulting laser intensities inside the films. The thin-film structure should not change with the increasing  $\text{HfO}_2$  layer thickness (the deposition conditions described above were selected to accomplish this goal); the total integrated  $\text{HfO}_2$  layer thickness should be the same for single-layer and multilayer films, and E-field intensities inside both types of film samples must be comparable (preferably very close in value). To fulfill these requirements,  $\text{HfO}_2$  single-layer films and  $\text{HfO}_2/\text{SiO}_2$  multilayer films were manufactured with a total  $\text{HfO}_2$  material optical thickness equal to one wave at 355 nm, which corresponds to a physical thickness of 174 nm. The multilayer film

was comprised of seven  $\text{HfO}_2$  layers, each 25 nm thick, separated by 17-nm-thick  $\text{SiO}_2$  layers (see Figs. 145.42 and 145.43).

The thickness of the  $\text{SiO}_2$  layers in the multilayer film (seven-layer film for future reference) was optimized to produce an E-field peak and average intensity as close as possible to the E-field intensity in the single-layer film (see Fig. 145.44). High-resolution transmission electron microscopy (TEM) along with x-ray diffraction (XRD) analysis (depicted in Fig. 145.45) reveals a fully amorphous, highly homogeneous film structure for both the seven-layer and single-layer sputtered films. The seven-layer film's interfaces [Fig. 145.45(a)] are sharp, have a roughly estimated width of 2 nm to 4 nm, and indicate no locally increased defect density. The e-beam-evaporated films were also mostly amorphous, but interfaces were not as clearly defined compared to the sputtered films [see Fig. 145.43(c)].

The coatings were deposited on polished fused-silica substrates with a 500-nm-thick  $\text{SiO}_2$  layer that served as an

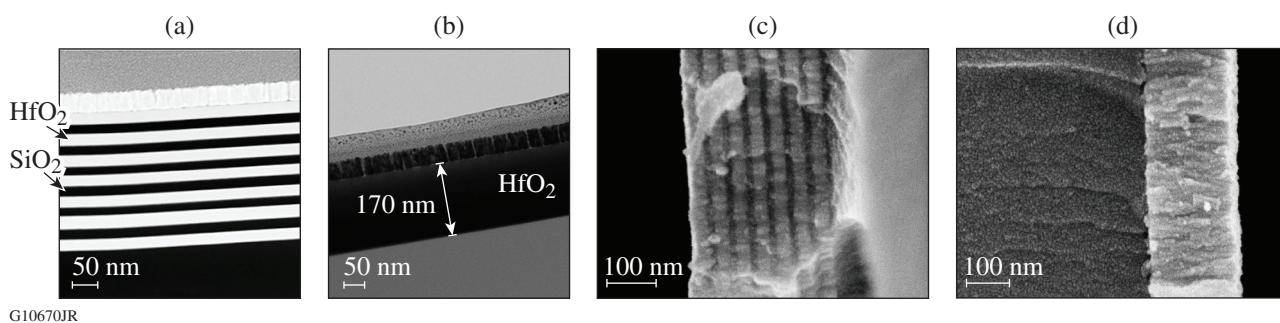


Figure 145.43

Transmission electron microscopy (TEM) images of sputtered  $\text{HfO}_2$  films: (a) seven layer and (b) single layer. The top-most conductive layer in (a) and (b) is for TEM imaging purposes only. Electron microscopy images of electron-beam-deposited  $\text{HfO}_2$  films: (c) seven layer and (d) single layer.

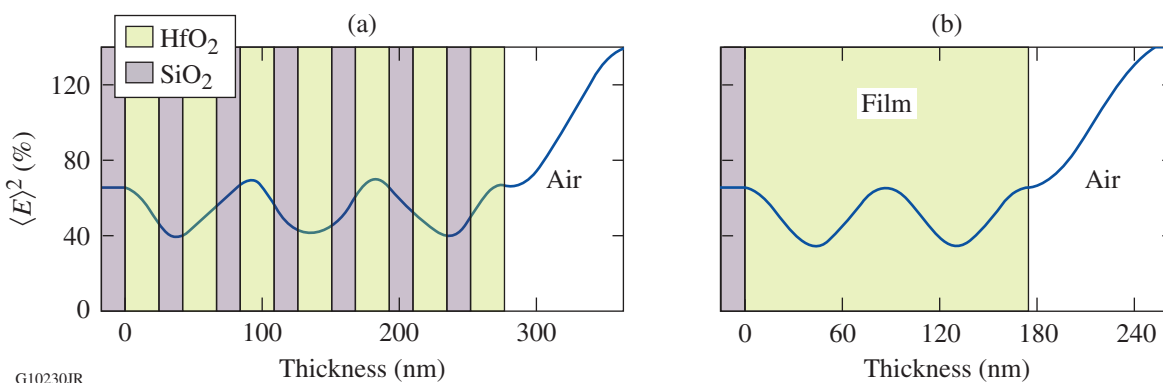


Figure 145.44

E-field intensity distribution in (a) seven-layer and (b) single-layer films.

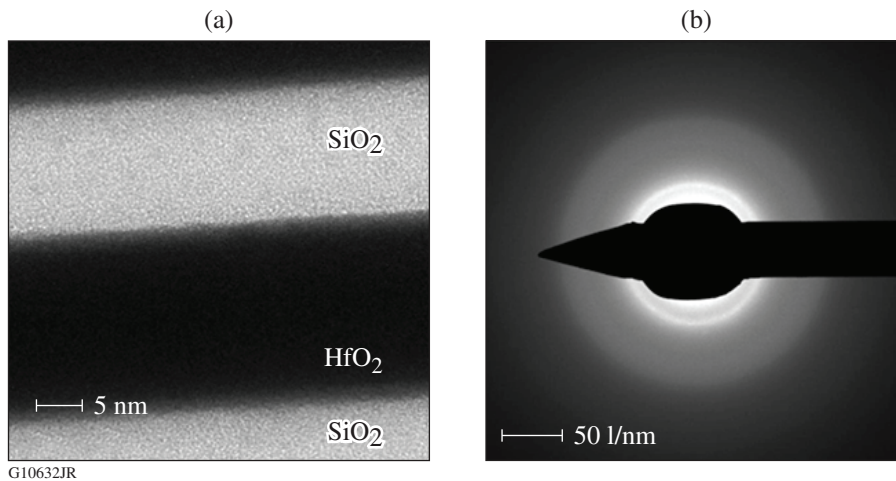


Figure 145.45

(a) A high-resolution TEM image of a seven-layer sputtered film shows a homogeneous structure with sharp interfaces and no evidence of local increased defect density. (b) X-ray diffraction (XRD) analysis confirmed a fully amorphous structure in both types of sputtered film.

insulator from defects introduced into the substrate during the finishing process. While not fully suppressing damage initiation by these defects, introducing such an additional  $\text{SiO}_2$  layer leads to distinct substrate defect-driven damage morphology, which could be easily separated from damage initiated inside the  $\text{HfO}_2$  film or interfaces (see **Damage Thresholds**, p. 46).

The absorption of the samples was characterized using a continuous-wave, 355-nm laser along with the following two methods: laser calorimetry (LC) and photothermal heterodyne imaging (PHI). The LC method detects heat generated through absorption of laser light and conducted by the film to the calibrated detector located on the front sample surface.<sup>5,6</sup> This method delivers absolute absorption values with good accuracy. The PHI method is a pump–probe laser technique based on the scattering of the probe light caused by local heating of the material by a tightly focused modulated pump beam.<sup>7,8</sup> The PHI method has high sensitivity and submicron spatial resolution but is more suitable for relative measurements because it is very difficult to achieve absolute calibration. Also, since this method is based on modulation of the refractive index of the material, it might be sensitive to the presence of different materials in the multilayer film. For that reason, we will consider LC as the main method of absorption characterization and PHI only as a complementary method.

Laser irradiation of samples was conducted mostly in a 1-on-1 regime (single-pulse irradiation of each sample site) using either 351-nm, 1-ns pulses [at the Laboratory for Laser Energetics (LLE)] or 355-nm, 5-ns pulses [at the Laser Zentrum Hannover (LZH) facility]. The 5-ns pulses were also used with 100-Hz frequency for the multipulse irradiation testing (10,000 pulses in this case) of each site at a fixed laser fluence. In addition, to probe changes in the interfacial structure as compared to the  $\text{HfO}_2$  film

structure (see **Femtosecond Damage Behavior as a Sensitive Tool to Detect Structural Changes and Its Application to  $\text{HfO}_2/\text{SiO}_2$  Interfaces**, p. 49), single-pulse irradiation with 1053-nm, 600-fs pulses was conducted for both types of samples in vacuum (to avoid the self-focusing effects in air). Damage was detected using 110 $\times$ -magnification dark-field microscopy or 150 $\times$ -magnification Nomarsky microscopy. Laser-damage morphology was further investigated using atomic force microscopy (AFM) and scanning laser microscopy (SLM) as high-resolution tools. The high-spatial-resolution study of damage morphology was essential for separating the contribution to damage from film defects and defects residing in a subsurface layer of the substrate. The latter defects gave rise to large damage craters of up to  $\sim 10\ \mu\text{m}$  in diameter, which, after high-resolution mapping, were excluded from damage statistics.

## Results and Discussion

### 1. Absorption Measurements

Absorption-measurement data may provide guidance for anticipated optical losses in the laser system and, in some cases, for nanosecond-pulse damage performance of  $\text{HfO}_2$  films.<sup>8</sup> For this study, the total contribution to near-UV absorption in the seven-layer film can come from two sources: structural defects in  $\text{HfO}_2$  layers of the film and defects residing within the interfacial structure (absorption inside  $\text{SiO}_2$  layers is negligibly small).

Considering additivity, total absorption  $A_{\text{total}}$  may be presented as follows:  $A_{\text{total}}^7 = A_{\text{HfO}_2} + A_{\text{interface}}$  for the seven-layer film, and  $A_{\text{total}}^1 = A_{\text{HfO}_2}$  for the single-layer film, where the superscripts 7 and 1 represent seven-layer and single-layer films, respectively.

Consequently, since the total thickness of seven hafnia layers is equal to the thickness of the single-layer film, a large-enough

contribution from interfaces should result in a larger total absorption for the seven-layer film as compared to the single-layer film. Absorption-measurement results are summarized in Table 145.V.

LC measurement results show, within a margin of error, nearly equal absorption in both seven-layer and single-layer film samples and almost two times higher absorption in the single-layer e-beam film as compared to seven-layer film. This result points to an insignificant contribution to absorption from interfaces.

The PHI method shows an even smaller relative absorption for a seven-layer film containing numerous interfaces that might be partially attributed (as discussed in **Experimental**, p. 43) to different conditions for signal formation (not just absorption) in single-layer and seven-layer films. Still, a 50% difference in the case of sputtered films and an even higher ratio for e-beam films indicates a small contribution from interfaces.

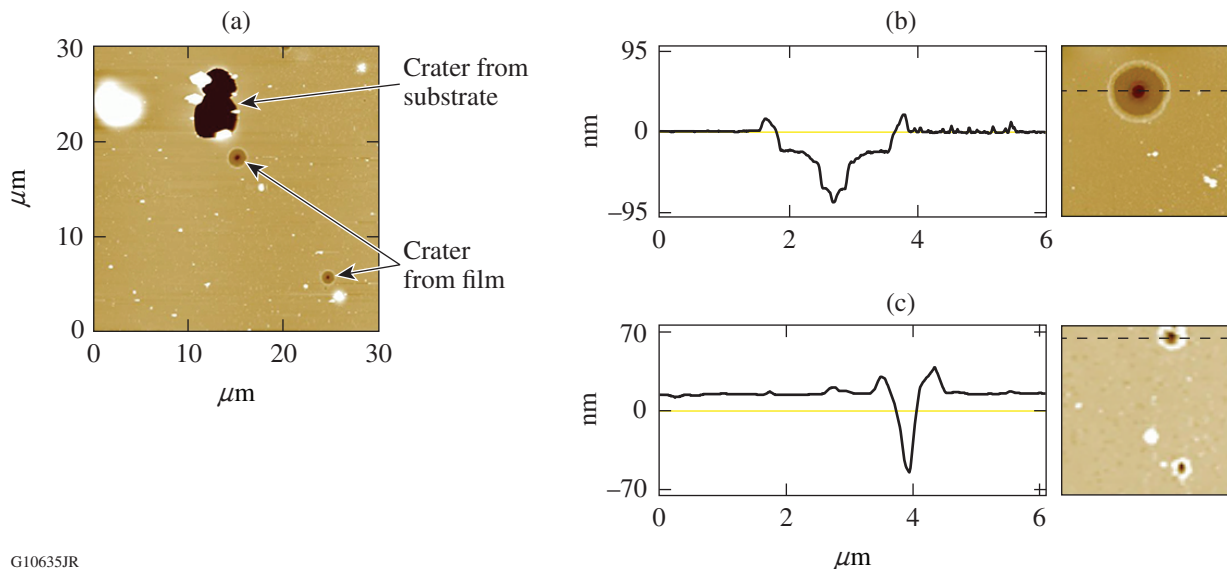
## 2. Damage Thresholds

The transparent nature of the coatings involved in this study required the careful separation of damage originating from film volume (seven-layer film or single-layer film) and from substrate–subsurface defects introduced during the substrate-finishing process. The presence of an isolating 500-nm-thick  $\text{SiO}_2$  layer (see Fig. 145.42) leads to much deeper and larger damage craters initiated by substrate defects, compared to craters formed by absorption inside the  $\text{HfO}_2$  layers. AFM mapping clearly reveals this difference (see Figs. 145.46 and 145.47) and allows one to exclude craters initiated by substrate defects from damage statistics.

To find the 351-nm, 1-ns damage threshold, ten sample sites were irradiated with a different laser fluence, and subsequent AFM mapping enabled us to acquire the damage-crater statistics depicted in Fig. 145.48. The thresholds were obtained by

Table 145.V: The 355-nm absorptance of seven-layer and single-layer films measured by laser calorimetry (LC) and photo-thermal heterodyne imaging (PHI) signals produced with a 355-nm pump laser.

Film type	LC (%)		PHI signal ( $\mu\text{V}$ )	
	Ion beam	e-beam	Ion beam	e-beam
Seven layers	$0.14 \pm 0.01$	$0.015 \pm 0.001$	$31.5 \pm 0.5$	$0.24 \pm 0.10$
Single layer	$0.13 \pm 0.01$	$0.027 \pm 0.002$	$47.0 \pm 0.5$	$1.28 \pm 0.16$



G10635JR

Figure 145.46

Atomic force microscopy mapping of damage morphology in sputtered films: (a)  $30 \times 30\text{-}\mu\text{m}$  image of the seven-layer film. Large ( $\sim 10\text{-}\mu\text{m}$ -diam) craters originate from a location corresponding to substrate–subsurface defects and much smaller ( $\leq 2\text{-}\mu\text{m}$ -diam) craters originate from the film volume; (b) cross-sectional profile through a crater originating inside the seven-layer film; (c) cross-sectional profile through a crater originating inside the single-layer film.

linear fitting and extrapolation of the trend line to the fluence at which the number of craters is equal to zero. It should be noted that in the case of the e-beam-deposited, seven-layer film, only the upper limit of the threshold value was estimated because of collateral damage caused by substrate defects at laser fluences exceeding  $8 \text{ J/cm}^2$ . Below this fluence level no craters originating from the film volume were found using AFM mapping.

In the case of 355-nm, 5-ns pulse irradiation, damage morphology was analyzed using  $150\times$ -magnification optical microscopy and, for crater profiling, SLM (see Fig. 145.49). Similar to AFM mapping, SLM analysis made it possible to separate the damage originating within the film volume from the substrate-defect-driven damage. Damage thresholds were obtained from the damage probability curves shown in

Fig. 145.50. The threshold measurement results are summarized in Table 145.VI.

The thresholds increase only marginally with the pulse-length increase (practically no scaling), which might be explained by different methodology used to derive the thresholds at the two

Table 145.VI: Damage thresholds of ion-beam-sputtered and e-beam-evaporated films.

Film type	Thresholds ( $\text{J/cm}^2$ )		
	351 nm, 1 ns		355 nm, 5 ns
	Ion beam	e-beam	Ion beam
Single layer	$5.5 \pm 0.3$	$4.5 \pm 0.3$	$6.2 \pm 0.5$
Seven layer	$6.5 \pm 0.3$	$\geq 8$	$7.5 \pm 0.5$

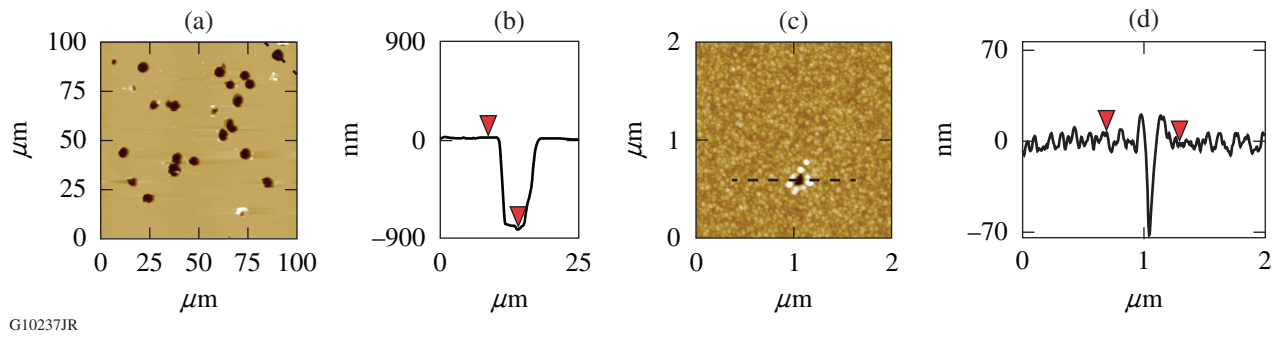


Figure 145.47

Atomic force microscopy mapping of damage morphology in e-beam-deposited films: (a)  $100 \times 100\text{-}\mu\text{m}$  image of the seven-layer film irradiated with a  $5.9\text{-J/cm}^2$  fluence. Damage morphology is dominated by craters initiated by substrate defects; (b) cross-sectional profile through a typical crater showing depth corresponding to substrate-subsurface absorbing-layer location ( $\sim 800 \text{ nm}$ ); (c)  $2 \times 2\text{-}\mu\text{m}$  image of the single-layer film irradiated with a  $4.6\text{-J/cm}^2$  fluence, which shows a crater originating from within the  $\text{HfO}_2$  film volume; and (d) cross-sectional profile through the crater shown in (c).

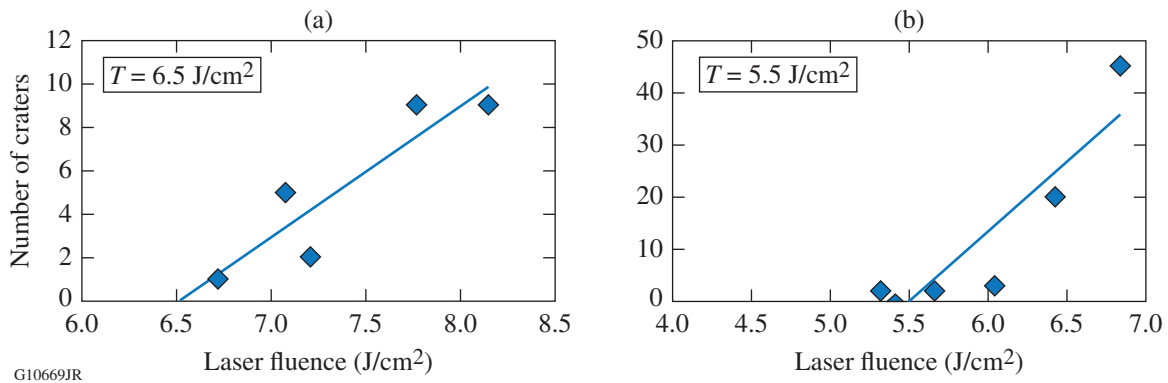
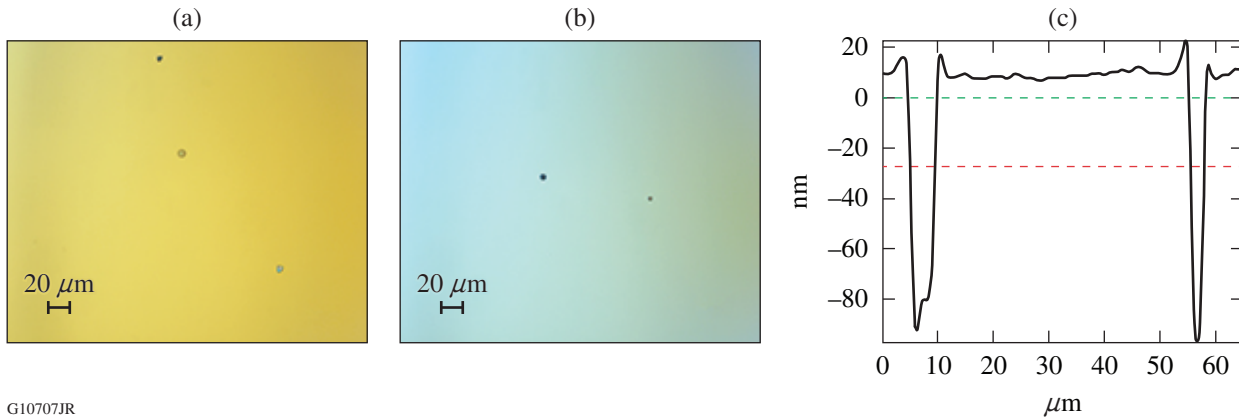
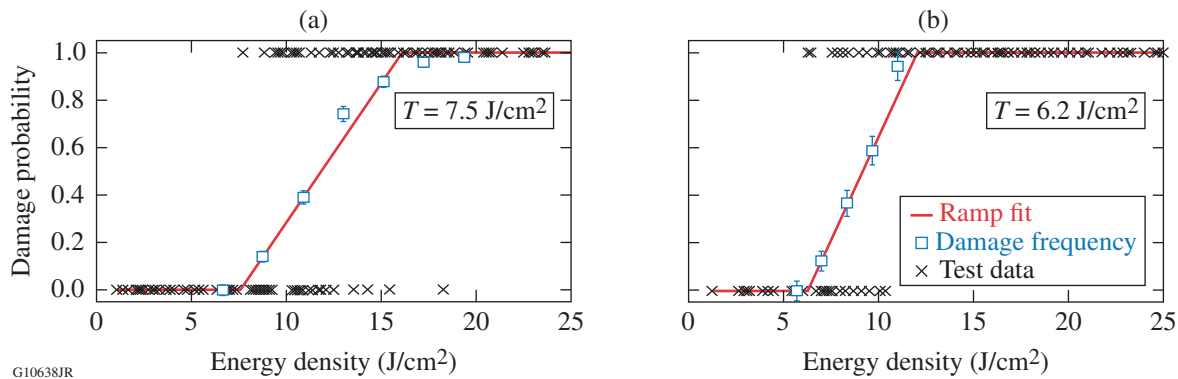


Figure 145.48

The number of damage craters originating from sputtered  $\text{HfO}_2$  films as a function of 351-nm, 1-ns laser fluence for (a) seven-layer and (b) single-layer films. The thresholds are obtained by linear extrapolation to the fluence at which the number of craters is equal to zero.



G10707JR  
 Figure 145.49  
 Optical microscope images of damage morphology of sputtered films irradiated at close-to-threshold conditions: (a) seven-layer film irradiated at  $7.7 \text{ J/cm}^2$  and (b) single-layer film irradiated at  $6.3 \text{ J/cm}^2$ . (c) An example of crater cross-sectional analysis using scanning laser microscopy (SLM).



G10638JR  
 Figure 145.50  
 Damage-probability curves resulting from 355-nm, 5-ns irradiation of sputtered films: (a) seven-layer and (b) single-layer film. The thresholds are obtained by a linear extrapolation to zero probability.

different facilities (LLE and LZH). More importantly, these results obtained for thin films with distinctly different morphology—densely packed ion-beam-deposited films and highly porous e-beam films—demonstrate higher nanosecond-pulse damage resistance for the film containing numerous  $\text{HfO}_2/\text{SiO}_2$  interfaces as compared to a single-layer  $\text{HfO}_2$  film. Note that the E-field peak intensity in the seven-layer film is slightly ( $\sim 7\%$ ) higher than that in the single-layer film, which means that the threshold ratio normalized by internal intensity would be even higher. Also, at close-to-threshold conditions, only a few damage sites (craters) are initiated in the sputtered seven-layer film [see Fig. 145.48(a)], and at the same laser fluence of  $6.5 \text{ J/cm}^2$  the number of craters initiated in the single-layer film exceeds 20 [see Fig. 145.48(b)], therefore pointing to lower damage resistance of the single-layer film. All of these facts lead to the conclusion that  $\text{HfO}_2/\text{SiO}_2$  interfaces are not a source of enhanced

near-UV localized absorption and laser damage. One possible explanation for these findings comes from the hypothesis that the interfacial structure is similar to the film structure formed during co-deposition of  $\text{HfO}_2$  and  $\text{SiO}_2$ . It was convincingly demonstrated that in co-deposited films, near-UV absorption is reduced and damage resistance becomes higher in  $\text{HfO}_2$  films with an increased  $\text{SiO}_2$  content.<sup>9</sup>

### 3. E-Field Intensity Distribution and Damage Morphology

A correlation between E-field intensity inside a coating and damage initiation is well established. One example is damage originating in nodular-coating defects where a large E-field may be generated.<sup>10</sup> To test the presence of such a link in this study, crater-depth distributions obtained at  $\sim 70\%$  above threshold conditions using SLM (see Fig. 145.51) were compared to the E-field intensity distributions depicted in Fig. 145.44. One

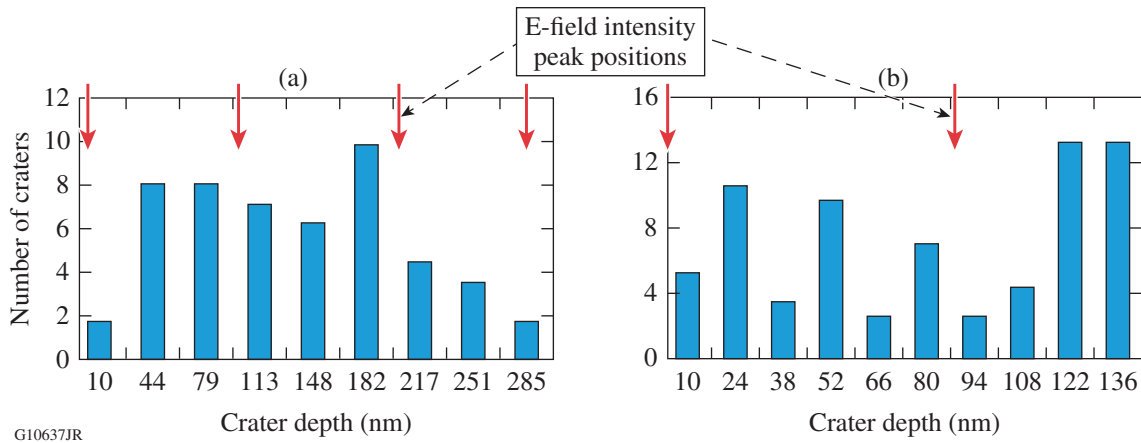


Figure 145.51 Crater-depth distributions obtained from SLM analysis for (a) seven-layer and (b) single-layer films.

can see that crater-depth distributions show no correlation with E-field peak positions; this observation does not change even when the depth bin size used to calculate the distribution is varied.

There are several reasons why a correlation was not observed: First, the intensity variation from the minimum to maximum value was not high for both types of film; the normalized intensity ( $|E|^2$ ) varied from 40% to 70% and from 34% to 65% in the seven-layer and single-layer films, respectively. For comparison, in standard quarter-wave reflectors,  $|E|^2$  might vary from 0% to 100% (Ref. 11). Second, crater depth depends not only on the location of the localized absorber but also on the amount of energy locally deposited,<sup>12</sup> which leads to a distribution in the crater-depth values.

#### 4. Femtosecond Damage Behavior as a Sensitive Tool to Detect Structural Changes and Its Application to $\text{HfO}_2/\text{SiO}_2$ Interfaces

The key to understanding the role of interfaces in pulsed laser damage is a knowledge of how the electronic structure changes during the spatial transition from  $\text{HfO}_2$  to  $\text{SiO}_2$  and vice versa. An important parameter here is a band gap of  $E_g$  and characteristics of the electronic defect states,<sup>13,14</sup> such as location in a gap (see Fig. 145.52), densities, and absorption coefficients. In the absence of structural data for interfaces, an alternative empirical approach is to study the interaction of subpicosecond laser pulses with optical materials—in this particular case, with a film containing numerous  $\text{HfO}_2/\text{SiO}_2$  interfaces and a single-layer  $\text{HfO}_2$  film. Femtosecond-pulse laser damage in dielectrics typically starts with the multiphoton ionization (MPI) process, which is very sensitive to band-gap

and defect-state characteristics.<sup>15,16</sup> The sensitivity is linked to a possible change in the number of absorbed photons required to promote an electron into the conduction band, which leads to a dramatic change in the multiphoton absorption coefficient.<sup>17</sup> Since the same defect states might participate in multiphoton absorption of infrared light and single-photon absorption of UV light (see Fig. 145.52), a femtosecond damage study may indicate whether an interfacial structure is more or less damage resistant than an  $\text{HfO}_2$  structure in the case of UV light and nanosecond pulses. In this study, the existence of such a correlation was tested by 1053-nm, 600-fs pulse irradiation (1-on-1 test) of single-layer and seven-layer samples. The damage thresholds  $T$ , normalized by internal E-field intensity

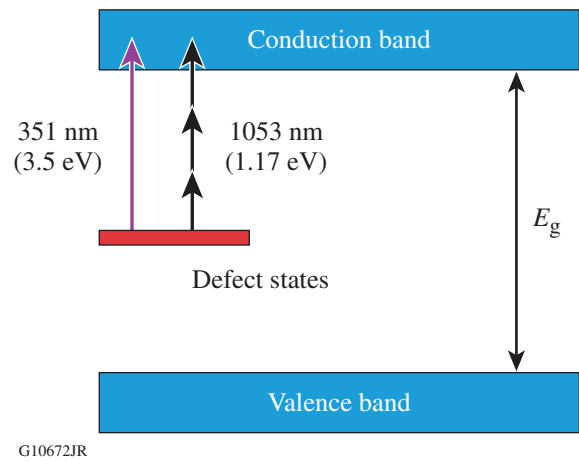


Figure 145.52 Schematic of the dielectric band structure with electronic defect states taking part in single-photon and multiphoton absorption promoting an electron into the conduction band.

[(average intensity was used for normalization because of slow changes across the film (see Fig.145.53)] showed a ratio of  $T_{\text{seven layer}}/T_{\text{single layer}} \geq 1.1$  for both ion-beam-sputtered and e-beam-evaporated films.

This result points to a low contribution of interfaces to the MPI process and correlates well with higher near-UV, nanosecond-pulse damage resistance of the interfacial structure as compared to the  $\text{HfO}_2$  film, in agreement with the 351-/355-nm threshold measurement results presented in **Damage Thresholds** (p. 46). This result also strongly supports the possibility that initial absorption—single photon for nanosecond pulses and multiphoton for femtosecond pulses—is initiated by the same structural defects.

### 5. Multipulse Irradiation

From a practical point of view, it is of interest to know how interfaces respond to multipulse, fixed-fluence irradiation. The typical behavior of coatings is characterized by the fatigue effect manifested by a lower threshold and increased scale of damage.<sup>18</sup> For this purpose, 10,000-pulse (355-nm, 5-ns) irradiation at a fixed laser fluence and a 100-Hz repetition rate was performed for seven-layer and single-layer films. The density of produced damage sites (craters) was calculated and compared with damage-site density produced using single-shot irradiation at a fluence slightly above the single-shot threshold. The fatigue effect was observed for both types of films but with a less-pronounced effect for the film with numerous interfaces. The seven-layer film showed a seven-fold increase in damage-site density compared to a 12-fold increase for a single-layer film. This result points to an interfacial structure that is less susceptible to absorbing-defect formation under near-UV light irradiation, as compared to the pure- $\text{HfO}_2$  material.

### Conclusions

The role of ion-beam-sputtered and e-beam-evaporated  $\text{HfO}_2/\text{SiO}_2$  film interfaces in near-UV absorption and nanosecond-pulse damage was investigated by comparing the damage performance of a film with numerous interfaces (seven  $\text{HfO}_2$  layers) and a monolayer  $\text{HfO}_2$  film. The films were characterized by an overall equal  $\text{HfO}_2$  material thickness, comparable E-field intensity, and fully amorphous material structure.

The study revealed a low contribution of interfaces to near-UV absorption and higher nanosecond-pulse damage thresholds for a film with numerous interfaces as compared to a single-layer  $\text{HfO}_2$  film. These results indicate that  $\text{HfO}_2/\text{SiO}_2$  interfacial structures have a higher laser-damage resistance than a structure of a pure  $\text{HfO}_2$  film.

The similarity of an interfacial  $\text{HfO}_2/\text{SiO}_2$  structure to a structure formed during co-deposition of  $\text{HfO}_2$  and  $\text{SiO}_2$  materials, which is documented to have higher pulsed-laser-damage resistance as compared to a pure  $\text{HfO}_2$  film material, may offer a possible explanation for these findings. A correlation found between near-UV, nanosecond-pulse and 1053-nm, 600-fs pulse damage of  $\text{HfO}_2$  coatings used for this study allows one to suggest that the initial absorption (single photon for nanosecond pulses and multiphoton for femtosecond pulses) involves the same electronic defect states. The relevance of these results to other high-/low-index film material pairs requires additional studies.

### ACKNOWLEDGMENT

This material is based upon work supported by the Department of Energy National Nuclear Security Administration under Award Number DE-NA0001944, the University of Rochester, and the New York State Energy Research and Development Authority. This work is also supported by the

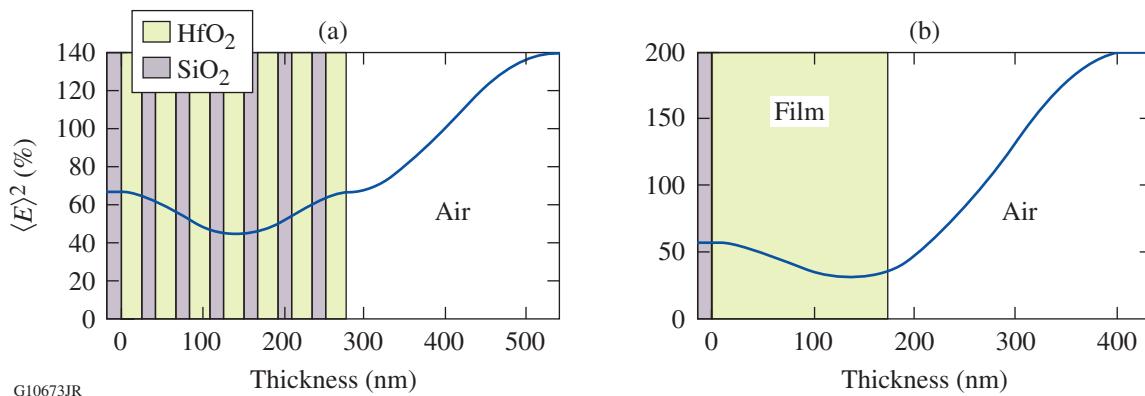


Figure 145.53  
The distribution of 1053-nm E-field intensity in (a) seven-layer and (b) single-layer films.

German Federal Ministry of Education and Research within Ultra-Life project under contract #13N11558. The support of DOE does not constitute an endorsement by DOE of the views expressed in this article.

## REFERENCES

1. J. H. Apfel, *Appl. Opt.* **16**, 1880 (1977).
2. D. H. Gill, B. E. Newnam, and J. McLeod, in *Laser Induced Damage in Optical Materials: 1977*, edited by A. J. Glass and A. H. Guenther, Nat. Bur. Stand. (U.S.), Spec. Publ. 509 (U.S. Government Printing Office, Washington, DC, 1977), pp. 260–270.
3. D. Ristau, X. C. Dang, and J. Ebert, in *Laser Induced Damage in Optical Materials: 1984*, edited by H. E. Bennett *et al.*, Natl. Bur. Stand. (U.S.), Spec. Publ. 727 (U.S. Government Printing Office, Washington, DC, 1986), pp. 298–306.
4. H. K. Pulker, in *Optical Interference Coatings*, edited by N. Kaiser and H. K. Pulker, Springer Series in Optical Sciences, edited by A. Adibi *et al.* (Springer-Verlag, Berlin, 2003), pp. 131–154.
5. U. Willamowski, D. Ristau, and E. Welsch, *Appl. Opt.* **37**, 8362 (1998).
6. I. Balasa, L. Jensen, and D. Ristau, *Proc. SPIE* **8885**, 88851L (2013).
7. S. Berciaud *et al.*, *Phys. Rev. B* **73**, 045424 (2006).
8. S. Papernov, A. Tait, W. Bittle, A. W. Schmid, J. B. Oliver, and P. Kupinski, *J. Appl. Phys.* **109**, 113106 (2011).
9. L. O. Jensen *et al.*, *Proc. SPIE* **7842**, 784207 (2010).
10. X. Cheng *et al.*, *Appl. Opt.* **53**, A62 (2014).
11. P. Baumeister, *Optical Coating Technology* (SPIE Optical Engineering Press, Bellingham, WA, 2004), pp. 9-56–9-57.
12. S. Papernov, in *Laser-Induced Damage in Optical Materials*, edited by D. Ristau (CRC Press/Taylor & Francis, Boca Raton, FL, 2014), Sec. I, Chap. 3, pp. 25–74.
13. A. S. Foster *et al.*, *Phys. Rev. B* **65**, 174117 (2002).
14. T.-J. Chen and C.-L. Kuo, *J. Appl. Phys.* **110**, 064105 (2011).
15. L. Gallais *et al.*, *Proc. SPIE* **8530**, 85300K (2012).
16. W. Rudolph *et al.*, *Proc. SPIE* **8885**, 888516 (2013).
17. L. V. Keldysh, *Sov. Phys.-JETP* **20**, 1307 (1965).
18. A. Hervy *et al.*, *Proc. SPIE* **9237**, 92370J (2014).